



Effect of titanium doping on conductivity, density of states and conduction mechanism in ZnO thin film

Arifa Jamil^{1,2} · S. Fareed³ · N. Tiwari⁴ · Chuanbo Li^{5,6} · Buwen Cheng⁵ · Xiulai Xu⁷ · M. A. Rafiq^{1,5} 

Received: 31 January 2019 / Accepted: 5 March 2019 / Published online: 7 March 2019
© Springer-Verlag GmbH Germany, part of Springer Nature 2019

Abstract

High quality, ~ 120 nm thin ZnO and Ti-doped ZnO (TZO) films were deposited on silicon substrates using magnetron co-sputtering technique. Surface roughness of the films was ~ 2 nm. Ti incorporation effect on the structure, morphology, conductivity, density of states (DOS) and conduction mechanism was investigated in detail. Ti ions were incorporated in the interstitial sites of hexagonal ZnO lattice. Average crystallite size increased from ~ 16.63 to ~ 19.08 nm upon Ti doping in ZnO film. Conduction mechanism changed from overlapping large polaron tunneling (OLPT) for undoped ZnO film to correlated barrier hopping (CBH) for TZO film. The experimental data were fitted theoretically using OLPT and CBH models to calculate frequency and temperature-dependent DOS. An enhancement of ac conductivity and DOS was observed with the doping of Ti in ZnO thin film. Complex modulus study of TZO film revealed transition from long-range mobility to short-range mobility with increase in frequency.

1 Introduction

Being nontoxic, inert, low cost and abundant material, zinc oxide (ZnO) has gained attention of research community [1–3]. In thin film form, the resistivity of undoped ZnO is due to electrons generated by Zn interstitial atoms and

oxygen vacancies and it may deteriorate. On the other hand, doped ZnO thin films have lower but stable resistivity [4].

Doping of ZnO also results in structural and microstructural modifications leading to improvement in performance [1]. For example, B, Al, Ga and In doping has been proved to decrease electrical resistivity of ZnO films [5–8]. In deciding the dopant atoms, it is important that the radius of the dopant atom is small or equal to that of the host atom. In view of this, Ti (radius of Ti = 0.68 Å and radius of Zn = 0.74 Å) atom seems to be suitable dopant for ZnO [9]. An initial study on Ti-, Sn- and Zr-doped ZnO also shows that crystal stability improves by Ti- dopant [10]. TZO films have shown lower resistivities and better optical properties [11–13].

Different techniques such as sputtering [4, 9], atomic layer deposition [14], chemical bath deposition [1], sol-gel process [15] and pulse laser deposition [2] have been utilized to prepare TZO thin films. Among these techniques, sputtering is suitable for composition control, uniformity, cleanness, large area deposition and deposition on different substrate materials [3, 11].

Therefore, we report effect of Ti doping in ZnO film on different film characteristics such conductivity, DOS and conduction mechanism. The thickness of the films was ~ 120 nm and was prepared using RF magnetron sputtering in conjunction with dc magnetron sputtering. Different relevant characterization tools were used to confirm the physical features, purity and chemical composition of the films. Then,

✉ M. A. Rafiq
aftab@cantab.net

¹ Department of Physics and Applied Mathematics, Institute of Engineering and Applied Sciences (PIEAS), P.O. Nilore, Islamabad 45650, Pakistan

² School of Materials Science and Engineering, Nanyang Technological University, Singapore 639798, Singapore

³ Department of Metallurgy and Materials Engineering, Institute of Engineering and Applied Sciences (PIEAS), P.O. Nilore, Islamabad 45650, Pakistan

⁴ Energy Research Institute (ERI), Nanyang Technological University (NTU), Singapore, Singapore

⁵ State Key Laboratory on Integrated Optoelectronics, Institute of Semiconductors, Chinese Academy of Sciences, Beijing 100083, China

⁶ School of Science, Minzu University of China, Beijing 100081, China

⁷ Beijing National Laboratory for Condensed Matter Physics, Institute of Physics, Chinese Academy of Sciences, Beijing 100190, China

detailed ac electrical measurements on ZnO and TZO films were carried out from 20 to 2 MHz at 203–303 K. To our knowledge, such studies on TZO films and their comparison with ZnO films have not been reported.

2 Experimental

Simultaneous RF and dc magnetron sputtering of 99.99% pure Ti and ZnO targets was used to deposit ~120 nm thick ZnO and TZO films. Before deposition, a background pressure of 3×10^{-6} torr was established and pre-sputtering for 15 min was carried out to expel possible contaminations. The sputtering was performed in argon atmosphere with working pressure of 2×10^{-2} torr. The substrate temperature was maintained at 20 °C for both ZnO and TZO films deposition. The typical RF and dc power was 80 W and 50 W, respectively, for deposition of TZO film. For deposition of ZnO film, ac power was 80 W and dc power was off. The Ti content in TZO film was 2 at% and was controlled by dc power. Two, $400 \times 400 \mu\text{m}$, Platinum contacts separated by 100 μm were also deposited on ZnO and TZO films for electrical measurements.

Film thickness measurements were carried out using surface profiler (Alpha-step IQ, KLA Tencor). The crystallographic structure of the ZnO and TZO films was investigated using X-ray diffraction (XRD) technique (Bruker D8 advance XRD). The surface morphology of prepared ZnO and TZO films was examined by asylum research atomic force microscope (AFM). The elemental composition of ZnO and TZO films was determined by Energy Dispersive Spectroscopy (EDS) using scanning electron microscope (JEOL JSM-6360). The ac electrical measurements of ZnO and TZO films were performed in a probe station using Agilent E4980A LCR meter.

3 Results and discussion

3.1 XRD and EDS analysis

Figure 1 shows the XRD patterns of undoped ZnO and TZO thin films indicating hexagonal wurtzite structure of the films. The patterns match with the JCPDS card No. 00-001-1136. The films have preferential growth in (002) direction (c-axis). From the XRD patterns, we note that (002) diffraction peak of TZO film slightly shifts towards lower diffraction angle as compared to undoped ZnO film. This shift is similar to the previous studies, carried on Ti-doped ZnO thin films [11, 16, 17]. Furthermore, full width at half maximum of the (002) peak decreases from 0.522 for undoped ZnO film to 0.455 for TZO film, suggesting that crystallinity improves after Ti-doping [18]. The average crystallite size

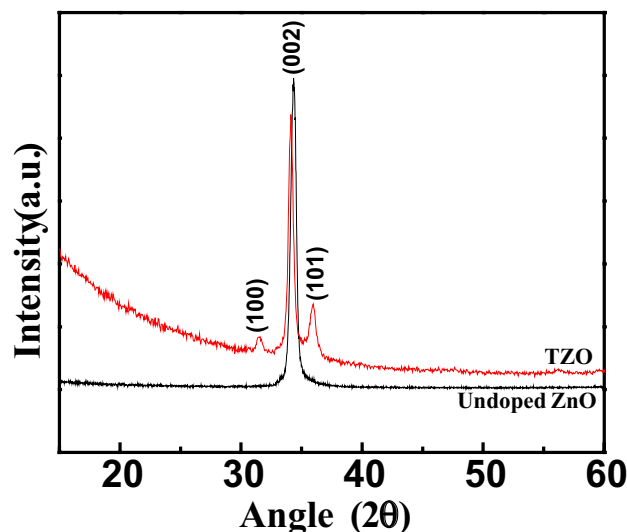


Fig. 1 XRD pattern of ZnO and TZO thin films

of the undoped ZnO and TZO films was calculated using the Scherrer's formula [19]. The increase in average crystallite size from ~16.63 to ~19.08 nm upon Ti doping in ZnO film implies better crystallization after Ti doping [18].

To evaluate the elemental composition of undoped ZnO and TZO films, EDS was performed and results are shown in Fig. 2a, b. Figure 2a indicates the presence of Zn and O only for undoped ZnO. However, Fig. 2b indicates the presence of Ti (2 at%) in addition to Zn and O in TZO film. The peak at 1.74 keV for ZnO and TZO films is due to Si substrate. No unwanted elements were detected in EDS spectrum. AFM images of undoped ZnO and TZO thin films are shown as an inset of Fig. 2a, b respectively. The films show dense, uniform and crack-free surface with spherical features with surface roughness ~2 nm.

3.2 Ac conductivity

The ac electrical measurements were performed to get information about different conductivity regions and conduction mechanisms [20] in undoped ZnO and TZO films. Figure 3a, b shows variation of real part of ac conductivity of undoped ZnO and TZO films with frequency from 203 to 303 K. The conductivity of the TZO thin film was greater than that of undoped ZnO film. This may be attributed to increase in charge carriers that result from Ti ions incorporation in the interstitial sites of ZnO lattice. Cherifi et al. [21] have also reported increase in conductivity by doping of Fe ions in ZnO. Slassi et al. calculated electrical conductivity of ZnO and Ti doped ZnO at 300 K using density functional theory. An increase in conductivity from $9.5 \Omega^{-1} \text{cm}^{-1}$ to $9.1 \times 10^3 \Omega^{-1} \text{cm}^{-1}$ was found due to the contribution of impurity states (Ti) around the fermi level

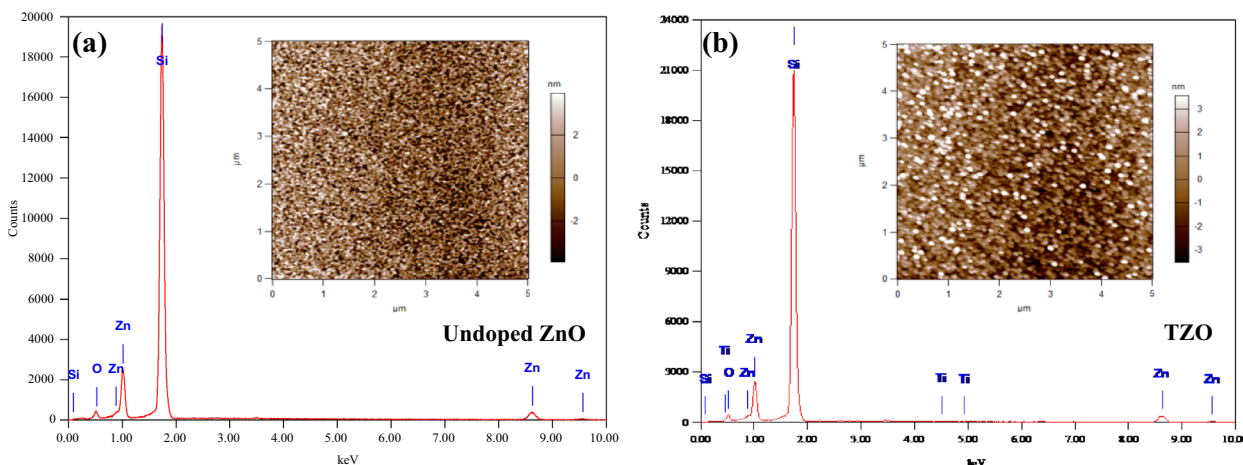
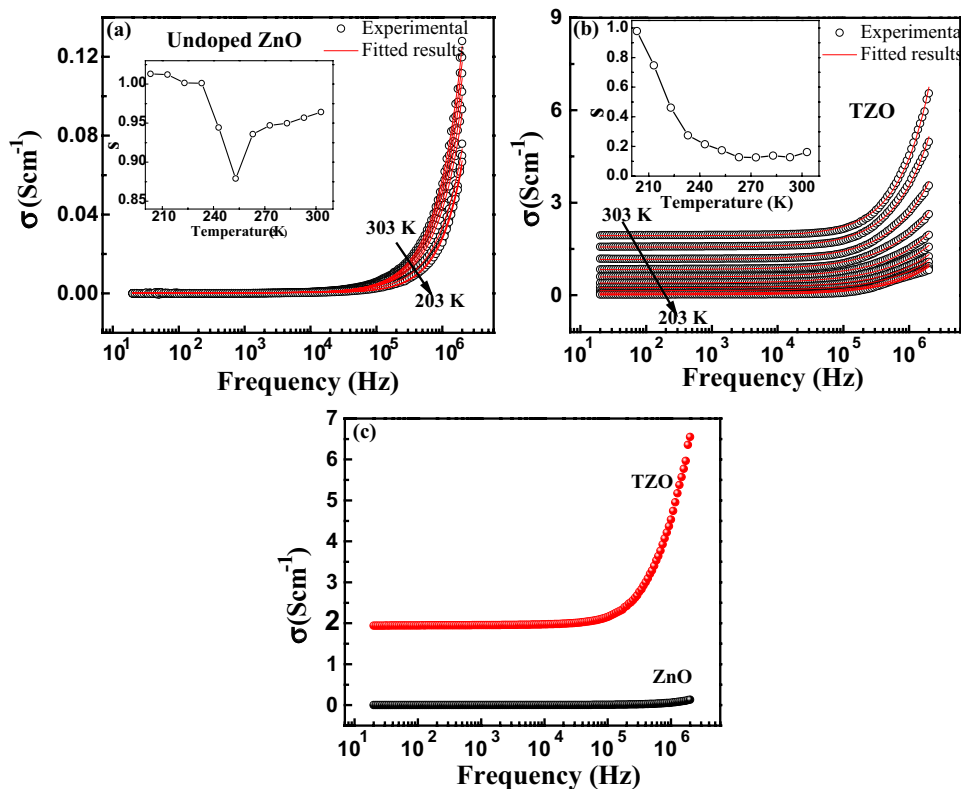


Fig. 2 EDS spectra of a undoped ZnO and b TZO thin films. Insets show AFM micrograph of the respective thin film

Fig. 3 The ac conductivity of a undoped ZnO and b TZO thin films. The insets show variation of the exponent s with temperature for the respective film. c The ac conductivity of ZnO and TZO at room temperature



[10]. This compliments our result where an increase in ac conductivity can be seen in Fig. 3 c with the incorporation of Ti in ZnO film at room temperature (303 K). The real part of ac conductivity is given as [22, 23]:

$$\sigma'_{ac} = \sigma_1(T) + \sigma_2(\omega, T), \tag{1}$$

The frequency-independent term σ_1 is dc conductivity due to free charge carriers. The frequency-dependent term σ_2 is

ac conductivity resulting due to free and bound charges and obeys Jonscher's power law [24]:

$$\sigma_2(\omega, T) = B(T)\omega^s(T), \tag{2}$$

where s shows the degree of interaction between mobile ions and lattices whereas B determines the strength of polarizability [25, 26]. Figure 3a, b shows electrical conduction of undoped ZnO and TZO thin films are thermally activated

[27]. As frequency of applied signal increases, ac conductivity of both films increases. The applied force on charge carriers increases at higher frequencies, as a result of which charge carriers liberate from various trapping states. It also facilitates charge carriers to transfer between different localized states [28, 29].

The exponent s was found by fitting Eq. 2 to the experimental data. The variation of s with temperature for ZnO and TZO films is shown as an inset of Fig. 3a, b. The parameter s determines the degree of order of a system. For an ordered system, $s < 1$ and $s > 1$ implies disorderness of the system [30, 31]. For undoped ZnO film $s > 1$ and for TZO film $s < 1$ indicating that Ti doping has increased order of ZnO film. A study of variation of s with temperature helps in determining type of conduction in a material. Generally observed types of conduction in a material include correlated barrier hopping (CBH) [32], small polaron conduction [33], overlapping large polaron tunneling (OLPT) [34] and quantum mechanical tunneling model [35]. For pure ZnO film, s drops when temperature rises, reaches a minimum value of 0.879 at 253 K and then rises again with increase in temperature as shown as an inset of Fig. 3a. This suggests that OLPT is prevailing conduction mechanism for ZnO thin film. For TZO thin film, CBH is the conduction mechanism as s decreases with increase in the temperature as shown as an inset of Fig. 3b.

3.2.1 OLPT model for ZnO thin film

A polaron is a charge surrounded by a distorted grid. The large polaron has radius greater than that of material’s lattice constants [27]. According to OLPT type of conductivity, Coulomb interactions appear in long range which results in overlapping of potential well of sites on one another [36, 37]. According to OLPT model, ac conductivity and exponent s are evaluated as [38, 39]:

$$\sigma(\omega) = \frac{\pi^4}{12} e^2 (k_B T)^2 [N(E_F)]^2 \frac{\omega R_\omega^4}{2\alpha k_B T + (r_p W_{HO}/R_\omega^2)} \quad (3)$$

Or

$$\sigma'(\omega) = \sigma_{dc} + \frac{\pi^4}{12} e^2 (k_B T)^2 [N(E_F)]^2 \frac{\omega R_\omega^4}{2\alpha k_B T + (r_p W_{HO}/R_\omega^2)} \quad (4)$$

and

$$s = 1 - \frac{8\alpha R_\omega + (6W_{HO}r_p/R_\omega k_B T)}{[2\alpha R_\omega + (W_{HO}r_p/R_\omega k_B T)]^2} \quad (5)$$

where R_ω , α , r_p , W_{HO} , and $N(E_f)$ are optimum polaron tunneling distance, inverse localization length, poron radius,

activation energy, and DOS, respectively. Equation 4 (OLPT model) was fitted well to the experimental data of ZnO film. The fitting process is restricted due to the limitation as two independent variables, namely ω and T , exist which may result in deviation from experimental data. To overcome this difficulty, we assume that $R\omega$ is negligibly dependent on frequency while performing the fitting process as reported in previous studies [40]. The obtained values after fitting procedure are $r_p = 1.414 \text{ \AA}$, $W_{HO} = 0.835 \text{ eV}$ and $\alpha = 0.784 \text{ \AA}^{-1}$. The values of R_ω lie in the range of 1.239–1.439 \AA . These values are similar to those obtained in previous studies [35, 38, 40].

$N(E_f)$ for ZnO thin film has been evaluated using Eq. 3. Frequency-dependent DOS at Fermi level $N(E_f)$ is presented in Fig. 4a from 203 to 303 K. Each plot shows a decrease in DOS with an increase in frequency up to $\sim 1 \text{ MHz}$ after which it starts to increase with an increase in frequency. A similar behavior of DOS with frequency was observed by Roy et al. where minima were obtained after which DOS

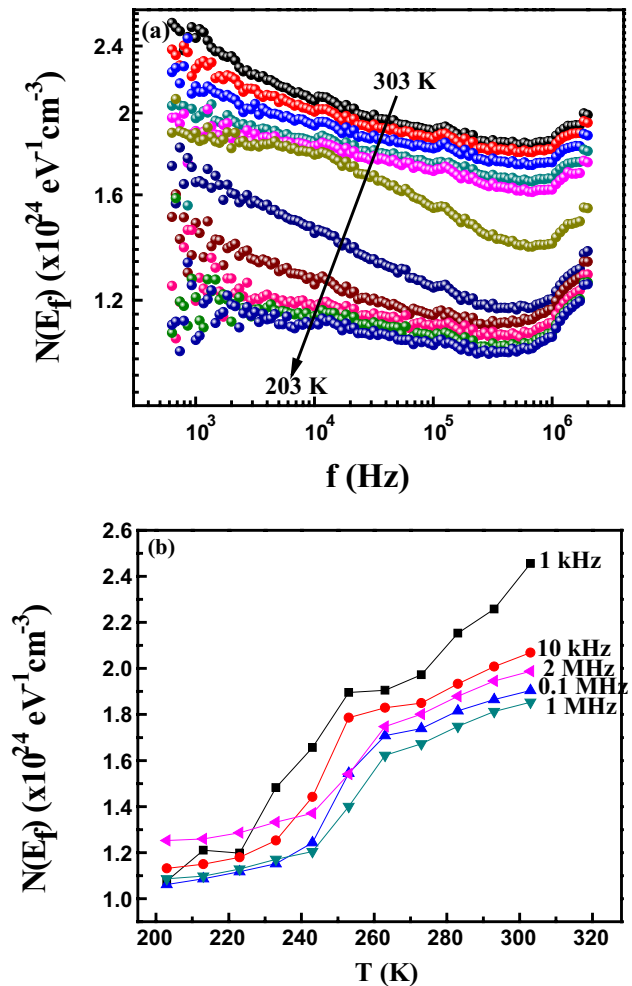


Fig. 4 a $N(E_f)$ vs Frequency and b $N(E_f)$ vs temperature plots for undoped ZnO thin film

increased with an increase in frequency [42]. Variation of $N(E_f)$ with temperature from 303 to 203 K at different frequencies is shown in Fig. 4b. Increase in temperature provides a contribution of thermal energy to polarons which subsequently moves and promotes the hopping resulting in an increase in $N(E_f)$ [37]. Lily et al. [43] and Prasad et al. [44] have observed similar trend in $N(E_f)$ for lead-free ceramics.

3.2.2 CBH model for TZO thin film

According to CBH model electrons hop over coulomb barrier between two site and the process is thermally activated. So short range translational hopping is the main cause of electrical conduction [27, 45]. The binding energy W_m is calculated by [43]:

$$s = 1 - \beta \tag{6}$$

where

$$\beta = 6k_B T / W_m \tag{7}$$

It is clear from above equation that binding energy of the system decreases as the temperature increases and, therefore, results in a decrease in slope as shown in the inset of Fig. 5c. This increases the number of free charge carriers having sufficient energy to overcome the barrier height and hence σ_{ac} increases with an increase in temperature. The minimum hopping distance R_{min} is [43]:

$$R_{min} = 2e^2 / \pi \epsilon_0 \epsilon W_m \tag{8}$$

where ϵ and ϵ_0 denote the dielectric constant and permittivity of free space respectively. Variation of R_{min} for TZO film with temperature at different frequencies is shown in Fig. 5a. A maxima is observed in R_{min} vs temperature plot at ~233 K which shifts towards low temperature as frequency decreases.

The ac conductivity has been used to calculate $N(E_f)$ for TZO using the relation [44]:

$$\sigma_{ac}(\omega) = \frac{\pi}{3} e^2 \omega k_B T \{N(E_f)\}^2 \alpha^{-5} \left\{ \ln \left(\frac{f_0}{\omega} \right) \right\}^4 \tag{9}$$

where f_0 and α are photon frequency and localized wave function, respectively, and $f_0 = 10^{13}$ Hz and $\alpha = 10^{10}$ m⁻¹ were used to calculate the DOS [42]. Figure 5b shows the variation of DOS $N(E_f)$ on frequency from 303 to 203 K. The DOS decreases with an increase in frequency at all temperatures. By decreasing temperature beyond 233 K, a maxima immediately appears after a minima at higher frequencies. Lily et al. also observed a minima which disappeared at higher temperatures in the study of the frequency dependence of $N(E_f)$ in lead-free ceramics [43]. Figure 5c illustrates the variation of $N(E_f)$ of TZO thin film from 303

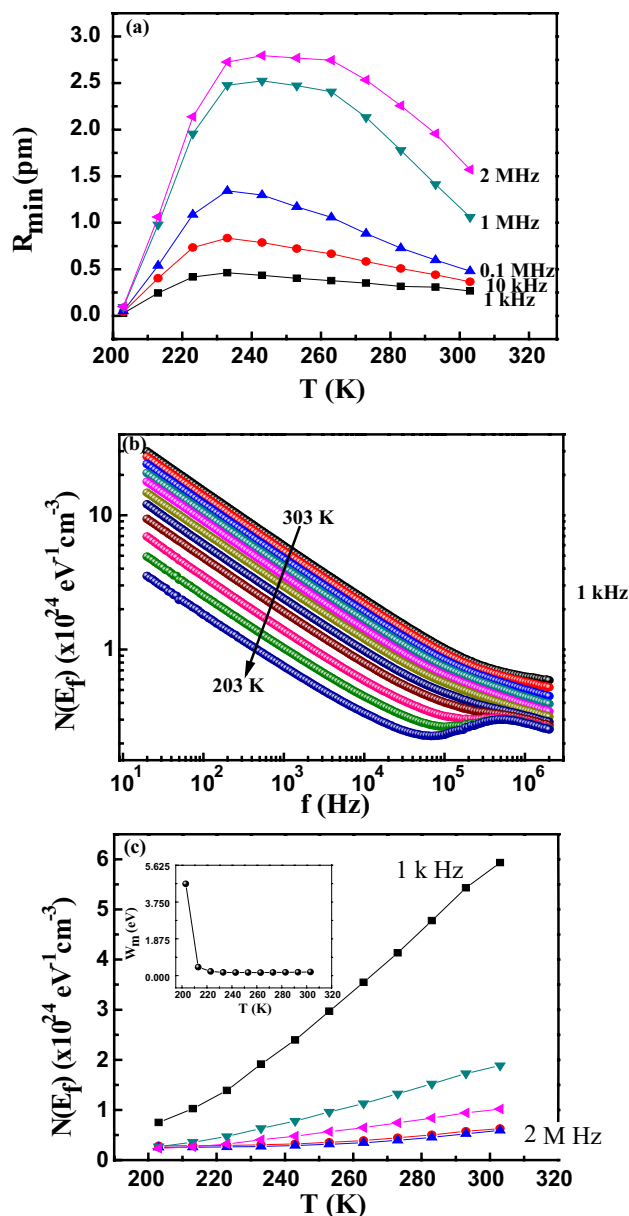


Fig. 5 a Temperature dependence of R_{min} at various frequencies for TZO film. b Frequency and c temperature dependence (at 1 kHz, 10 kHz, 0.1MHz, 1MHz, 2 MHz) of $N(E_f)$ for TZO thin film. Inset shows variation of binding energy with temperature

to 203 K at different frequencies. We note that DOS of TZO film increases with an increase in temperature for all frequencies. The high values of DOS propose that dominant charge transport mechanism is hopping between the pairs of sites in TZO thin film [43]. Density functional theory-based calculations have also demonstrated that doping creates shallow states mainly formed of Ti-4d states [10].

3.3 Modulus analysis

Complex electrical modulus (M^*) can be used to separate material components with similar resistances but different capacitances [25, 45, 46]. The $M^* = M' + jM''$ is the inverse of complex permittivity (ϵ^*) [47], where $M' = j\omega C_0 Z'$ is the real part of M^* and $M'' = j\omega C_0 Z''$ is the imaginary part of M^* , $\omega = 2\pi f$ is the angular frequency, $C_0 = \epsilon_0 A/t$ is the geometrical capacitance, t is the thickness, ϵ_0 is the permittivity of free space and A is the area of electrode surface [48]. Figure 6a shows frequency-dependent curves of M' in the temperature range 203–303 K for TZO thin film. At lower frequencies, the value of M' approaches to zero due to insufficient force governing mobility of charge carriers under applied electric field [49]. The value of M' close to zero suggests the suppression of the electrode polarization [50]. M' increases as applied frequency increases indicating saturation tendency at a maximum asymptotic value corresponding to $M_\infty = 1/\epsilon_\infty$ due to relaxation process [48, 50]. Furthermore, M' exhibits a decrease as temperature rises from 203 to 303 K which tells about temperature-dependent relaxation process in the TZO thin film.

The dependence of M'' on frequency from 303 to 203 K is plotted for TZO thin film in Fig. 6b–d. The M'' increases with an increase in frequency and attains maximum value in the temperature range 303–273 K. By further decreasing temperature up to 243 K, M'' first increases with frequency and then decreases so we attain a maximum. By further decreasing temperature up to 203 K, two maxima, one at lower frequency and second at higher frequency, were obtained. These two peaks (obtained at lower temperature) reveal that long range mobility changes to short-range mobility with an increase in frequency. The first peak at low frequencies is generally associated with interfacial polarization (grain boundaries) effects and the second peak at high frequencies is attributed to the dipolar polarization (grains effect) [50–53]. Thus, the presence of two peaks at lower temperature confirms the grain and grain boundary effects at lower temperatures and suppression of grains effect at higher temperatures for TZO thin film. Moreover, relaxation peak position moves towards higher frequencies as temperature increases. It suggests that relaxation rate for TZO thin film increases with temperature and hopping of charge carrier is the dominating mechanism [26]. Taher et al. express in

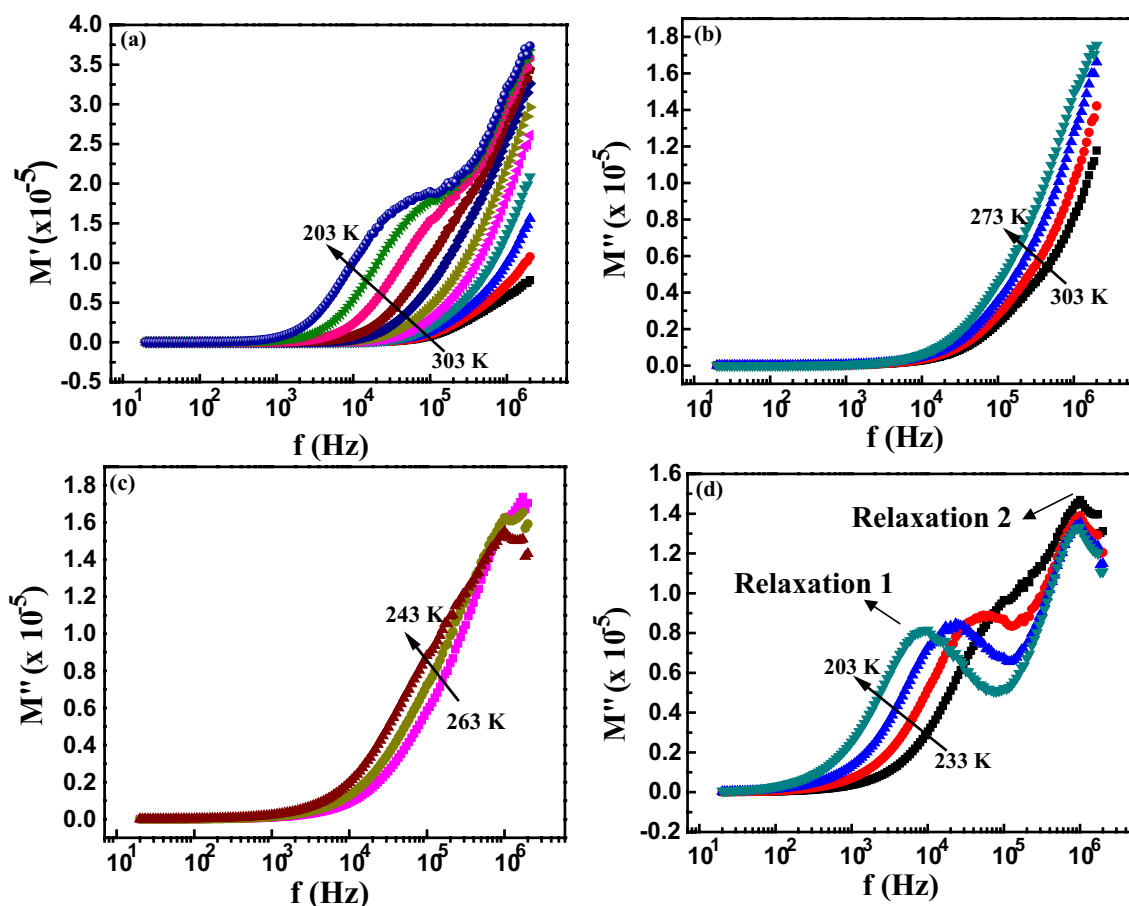


Fig. 6 Variation of a real and b–d imaginary modulus plots with frequency for TZO thin film from 303 to 203 K

their study that charge carriers move faster as temperature increases which leads to the reduction in relaxation time. As a result, peak shifts towards higher frequency with temperature [54].

4 Conclusions

Detailed comparative ac electrical measurements of ZnO and TZO thin films were carried out to explore conduction mechanisms, density of states and complex modulus properties. Magnetron co-sputtering technique was used for the deposition of films. The percentage of Ti in ZnO film was 2 at% and controlled by DC power of Ti target. XRD, EDS and AFM were used for structural and morphological analysis. An increase of greater than an order of magnitude in ac conductivity was observed for TZO thin film than that of undoped ZnO film. The OLPT and CBH are prevailing conduction mechanisms for ZnO and TZO thin film, respectively. DOS was calculated by fitting the theoretical OLPT and CBH models for ZnO and TZO thin films, respectively. In complex modulus study of TZO film, two relaxation peaks in the lower temperature range confirm the grain and grain boundary effects at lower temperatures and suppression of grains effect at higher temperatures.

Acknowledgements M. A. Rafiq would like to acknowledge Higher Education Commission for financial support under National Research Program for Universities (NRPU Project No 3662). M. A. Rafiq would also like to acknowledge the financial support from Chinese Academy of Sciences Presidents's International fellowship initiative grant No 2018VTA0002. A. Jamil would like to thank Higher Education Commission for financial support through IRSIP.

References

1. S.A. Bidier, M.R. Hashim, A.M. Al-Diabat, M. Bououdina, Effect of growth time on Ti-doped ZnO nanorods prepared by low-temperature chemical bath deposition. *Phys. E Low Dimens. Syst. Nanostruct.* **88**, 169–173 (2017). <https://doi.org/10.1016/J.PHYSE.2017.01.009>
2. W. Zhao, Q. Zhou, X. Zhang, X. Wu, A study on Ti-doped ZnO transparent conducting thin films fabricated by pulsed laser deposition. *Appl. Surf. Sci.* **305**, 481–486 (2014). <https://doi.org/10.1016/J.APSUSC.2014.03.119>
3. F.-H. Wang, J.-C. Chao, H.-W. Liu, T.-K. Kang, Physical properties of ZnO thin films codoped with titanium and hydrogen prepared by RF magnetron sputtering with different substrate temperatures. *J. Nanomater.* **2015**, 1–11 (2015). <https://doi.org/10.1155/2015/936482>
4. J.-L. Chung, J.-C. Chen, C.-J. Tseng, The influence of titanium on the properties of zinc oxide films deposited by radio frequency magnetron sputtering. *Appl. Surf. Sci.* **254**, 2615–2620 (2008). <https://doi.org/10.1016/J.APSUSC.2007.09.094>
5. M. Wang, Y. Zhang, H. Yu, Q. Li, S.H. Hahn, E.J. Kim, Nanosheet-constructed transparent conducting ZnO:In thin films. *J. Alloys Compd.* **561**, 211–213 (2013). <https://doi.org/10.1016/J.JALLCOM.2013.01.181>
6. P. Song, M. Watanabe, M. Kon, A. Mitsui, Y. Shigesato, Electrical and optical properties of gallium-doped zinc oxide films deposited by dc magnetron sputtering. *Thin Solid Films* **411**, 82–86 (2002). [https://doi.org/10.1016/S0040-6090\(02\)00192-X](https://doi.org/10.1016/S0040-6090(02)00192-X)
7. G. Kim, J. Bang, Y. Kim, S.K. Rout, S.I. Woo, Structural, electrical and optical properties of boron doped ZnO thin films using LSMCD method at room temperature. *Appl. Phys. A.* **97**, 821–828 (2009). <https://doi.org/10.1007/s00339-009-5317-9>
8. F.-H. Wang, H.-P. Chang, C.-C. Tseng, C.-C. Huang, Effects of H₂ plasma treatment on properties of ZnO:Al thin films prepared by RF magnetron sputtering. *Surf. Coat. Technol.* **205**, 5269–5277 (2011). <https://doi.org/10.1016/J.SURFCOAT.2011.05.033>
9. S.-S. Lin, J.-L. Huang, P. Šajgalik, The properties of Ti-doped ZnO films deposited by simultaneous RF and DC magnetron sputtering. *Surf. Coat. Technol.* **191**, 286–292 (2005). <https://doi.org/10.1016/J.SURFCOAT.2004.03.021>
10. A. Slassi, N. Lakouari, Y. Ziat, Z. Zarhri, A. Fakhim Lamrani, E.K. Hlil, A. Benyoussef, Ab initio study on the electronic, optical and electrical properties of Ti-, Sn- and Zr-doped ZnO. *Solid State Commun.* **218**, 45–48 (2015). <https://doi.org/10.1016/j.ssc.2015.06.010>
11. Y.-M. Lu, C.-M. Chang, S.-I. Tsai, T.-S. Wey, Improving the conductance of ZnO thin films by doping with Ti, *Thin Solid Films.* 447–448 (2004) 56–60. <https://doi.org/10.1016/J.TSF.2003.09.022>
12. Y.R. Park, K.J. Kim, Optical and electrical properties of Ti-doped ZnO films: observation of semiconductor–metal transition. *Solid State Commun.* **123**, 147–150 (2002). [https://doi.org/10.1016/S0038-1098\(02\)00217-X](https://doi.org/10.1016/S0038-1098(02)00217-X)
13. H. Chen, W. Guo, J. Ding, S. Ma, Ti-incorporated ZnO films synthesized via magnetron sputtering and its optical properties. *Superlattices Microstruct.* **51**, 544–551 (2012). <https://doi.org/10.1016/J.SPML.2012.02.003>
14. Z.-Y. Ye, H.-L. Lu, Y. Geng, Y.-Z. Gu, Z.-Y. Xie, Y. Zhang, Q.-Q. Sun, S.-J. Ding, D.W. Zhang, Structural, electrical, and optical properties of Ti-doped ZnO films fabricated by atomic layer deposition. *Nanoscale Res. Lett.* **8**, 108 (2013). <https://doi.org/10.1186/1556-276X-8-108>
15. M. Yilmaz, G. Turgut, Titanium doping effect on the characteristic properties of sol-gel deposited ZnO thin films. *Kov. Mater.* **53**, 333–339 (2015)
16. S.-S. Lin, J.-L. Huang, D.-F. Lii, Effect of substrate temperature on the properties of Ti-doped ZnO films by simultaneous rf and dc magnetron sputtering. *Mater. Chem. Phys.* **90**, 22–30 (2005). <https://doi.org/10.1016/J.MATCHEMPHYS.2004.08.040>
17. J.J. Lu, Y.M. Lu, S.I. Tasi, T.L. Hsiung, H.P. Wang, L.Y. Jang, Conductivity enhancement and semiconductor–metal transition in Ti-doped ZnO films. *Opt. Mater. Amst* **29**, 1548–1552 (2007). <https://doi.org/10.1016/J.OPTMAT.2006.08.002>
18. P.S. Shewale, N.K. Lee, S.H. Lee, K.Y. Kang, Y.S. Yu, Ti doped ZnO thin film based UV photodetector: Fabrication and characterization. *J. Alloys Compd.* **624**, 251–257 (2015). <https://doi.org/10.1016/J.JALLCOM.2014.10.071>
19. B.D. Cullity, *Elements of X-ray Diffraction*, 2nd ed., Addison-Wesley, New York 1978
20. R.D. Gould, A.K. Hassan, A. C. electrical properties of thermally evaporated thin films of copper phthalocyanine. *Thin Solid Films* **223**, 334–340 (1993). [https://doi.org/10.1016/0040-6090\(93\)90541-V](https://doi.org/10.1016/0040-6090(93)90541-V)
21. Y. Cherifi, A. Chaouchi, Y. Lorgoilloux, M. Rguiti, A. Kadri, C. Courtois, Electrical, dielectric and photocatalytic properties of Fe-doped ZnO nanomaterials synthesized by sol gel method. *Process. Appl. Ceram.* **10**, 125–135 (2016). <https://doi.org/10.2298/PAC1603125C>

22. M.F. Afsar, A. Jamil, M.A. Rafiq, Ferroelectric, dielectric and electrical behavior of two-dimensional lead sulphide nanosheets. *Adv. Nat. Sci. Nanosci. Nanotechnol.* **8**, 045010 (2017). <https://doi.org/10.1088/2043-6254/aa8b3d>
23. M. Ahmad, M.A. Rafiq, M.M. Hasan, Transport characteristics and colossal dielectric response of cadmium sulfide nanoparticles. *J. Appl. Phys.* **114**, 133702 (2013). <https://doi.org/10.1063/1.4823810>
24. A. K. Jonscher, The “universal” dielectric response, *Nature* **267** (1977) 673–679
25. J. Nagaraju, S. B. Krupanidhi, Dc and ac transport properties of Mn-doped ZnO thin films grown by pulsed laser ablation. *Mater. Sci. Eng. B.* **133**, 70–76 (2006). <https://doi.org/10.1016/J.MSEB.2006.05.005>
26. A. Tabib, N. Sdiri, H. Elhouichet, M. Férid, Investigations on electrical conductivity and dielectric properties of Na doped ZnO synthesized from sol gel method. *J. Alloys Compd.* **622**, 687–694 (2015). <https://doi.org/10.1016/j.jallcom.2014.10.092>
27. M. Krimi, K. Karoui, A. Ben Rhaiem, Electrical and dielectric properties of the Li_{1.5}Na_{0.5}WO₄ compound. *J. Alloys Compd.* **698**, 510–517 (2017). <https://doi.org/10.1016/J.JALLCOM.2016.12.237>
28. S. Fareed, A. Jamil, M.A. Rafiq, F. Sher, Zinc modified cadmium titanite nanoparticles: Electrical and room temperature methanol sensing properties. *Ceram. Int.* **44**, 4751–4757 (2018). <https://doi.org/10.1016/j.ceramint.2017.12.059>
29. A. Jamil, S.S. Batool, F. Sher, M.A. Rafiq, Determination of density of states, conduction mechanisms and dielectric properties of nickel disulfide nanoparticles. *AIP Adv.* **6**, 055120 (2016). <https://doi.org/10.1063/1.4952966>
30. M. Shunmugam, H. Gurusamy, P. Anand, Devarajan, Investigations on the structural, electrical properties and conduction mechanism of CuO nanoflakes. *Int. J. Nano Dimens.* **8**, 216–223 (2017)
31. S. Karthickprabhu, G. Hirankumar, A. Maheswaran, R.S. Daries Bella, C. Sanjeeviraja, Structural and electrical studies on Zn²⁺ doped LiCoPO₄. *J. Electrostat.* **72**, 181–186 (2014). <https://doi.org/10.1016/J.ELSTAT.2014.02.001>
32. M. Ganaie, M. Zulfeqar, Ac conductivity measurement of Cd₅Se_{95-x}Zn_x chalcogenide semiconductor using correlated barrier hopping model. *Acta Phys. Pol. A.* **128**, 59–63 (2015). <https://doi.org/10.12693/APhysPolA.128.59>
33. T.M. Meaz, S.M. Attia, A.M. Abo El, Ata, Effect of tetravalent titanium ions substitution on the dielectric properties of Co–Zn ferrites. *J. Magn. Magn. Mater.* **257**, 296–305 (2003). [https://doi.org/10.1016/S0304-8853\(02\)01212-X](https://doi.org/10.1016/S0304-8853(02)01212-X)
34. A. Ghosh, Ac conduction in iron bismuthate glassy semiconductors. *Phys. Rev. B* **42**, 1388–1393 (1990). <https://doi.org/10.1103/PhysRevB.42.1388>
35. I.G. Austin, N.F. Mott, Polarons in crystalline and non-crystalline materials. *Adv. Phys.* **18**, 41–102 (1969). <https://doi.org/10.1080/00018736900101267>
36. A. Jamil, M.F. Afsar, F. Sher, M.A. Rafiq, Temperature and composition dependent density of states extracted using overlapping large polaron tunnelling model in Mn_xCo_{1-x}Fe₂O₄ (x = 0.25, 0.5, 0.75) nanoparticles. *Phys. B Condens. Matter.* **509**, 76–83 (2017). <https://doi.org/10.1016/j.physb.2017.01.005>
37. N. Chakchouk, B. Louati, K. Guidara, Electrical properties and conduction mechanism study by OLPT model of NaZnPO₄ compound. *Mater. Res. Bull.* **99**, 52–60 (2018). <https://doi.org/10.1016/J.MATERRESBULL.2017.10.046>
38. M. Tan, Y. Köseoğlu, F. Alan, E. Şentürk, Overlapping large polaron tunneling conductivity and giant dielectric constant in Ni_{0.5}Zn_{0.5}Fe_{1.5}Cr_{0.5}O₄ nanoparticles (NPs). *J. Alloys Compd.* **509**, 9399–9405 (2011). <https://doi.org/10.1016/j.jallcom.2011.07.063>
39. R. Punia, R.S. Kundu, M. Dult, S. Murugavel, N. Kishore, Temperature and frequency dependent conductivity of bismuth zinc vanadate semiconducting glassy system. *J. Appl. Phys.* **112**, 083701 (2012). <https://doi.org/10.1063/1.4759356>
40. M.M. Abdel-Kader, M.A.F. Basha, G.H. Ramzy, A.I. Aboud, Thermal and ac electrical properties of N-methylantranilic acid below room temperature. *J. Phys. Chem. Solids* **117**, 13–20 (2018). <https://doi.org/10.1016/J.JPCS.2018.02.007>
41. S. Dahiya, R. Punia, S. Murugavel, A.S. Maan, Structural and other physical properties of lithium doped bismuth zinc vanadate semiconducting glassy system. *J. Mol. Struct.* **1079**, 189–193 (2015). <https://doi.org/10.1016/j.molstruc.2014.09.047>
42. A.K. Roy, A. Singh, K. Kumari, K. Amar Nath, A. Prasad, K. Prasad, Electrical Properties and AC Conductivity of (Bi_{0.5}Na_{0.5})_{0.94}Ba_{0.06}TiO₃ Ceramic, *ISRN Ceram.* **2012** (2012) 1–10. <https://doi.org/10.5402/2012/854831>
43. K. Lily, K. Kumari, R.N.P. Prasad, Choudhary, Impedance spectroscopy of (Na_{0.5}Bi_{0.5})(Zr_{0.25}Ti_{0.75})O₃ lead-free ceramic. *J. Alloys Compd.* **453**, 325–331 (2008). <https://doi.org/10.1016/j.jallcom.2006.11.081>
44. K. Prasad, K. Lily, K.P. Kumari, K.L. Chandra, S. Yadav, Sen, Electrical properties of a lead-free perovskite ceramic: (Na_{0.5}Sb_{0.5})TiO₃. *Appl. Phys. A.* **88**, 377–383 (2007). <https://doi.org/10.1007/s00339-007-3989-6>
45. M.A. Diab, N.A. El-Ghamaz, F.S. Mohamed, E.M. El-Bayoumy, Conducting polymers VIII: Optical and electrical conductivity of poly(bis-m-phenylenediaminosulphoxide). *Polym. Test.* **63**, 440–447 (2017). <https://doi.org/10.1016/J.POLYMERTESTING.2017.09.001>
46. S. Thakur, R. Rai, I. Bdkin, M.A. Valente, Impedance and modulus spectroscopy characterization of Tb modified Bi_{0.8}A_{0.1}Pb_{0.1}Fe_{0.9}Ti_{0.1}O₃ ceramics. *Mater. Res.* **19**, 1–8 (2016). <https://doi.org/10.1142/S0219720012030011>
47. M. Coskun, O. Polat, F.M. Coskun, Z. Durmus, M. Çağlar, A. Turut, The electrical modulus and other dielectric properties by the impedance spectroscopy of LaCrO₃ and LaCr_{0.90}Ir_{0.10} perovskites. *RSC Adv.* **8**, 4634 (2018). <https://doi.org/10.1039/C7RA13261A>
48. Z. Imran, M.A. Rafiq, M. Ahmad, K. Rasool, S.S. Batool, M.M. Hasan, Temperature dependent transport and dielectric properties of cadmium titanate nanofiber mats. *AIP Adv.* **3**, 032146 (2013). <https://doi.org/10.1063/1.4799756>
49. M.H. Lakhdar, T. Larbi, B. Khalfallah, B. Ouni, M. Amlouk, Structural, dielectric and a.c. conductivity study of Sb₂O₃ thin film obtained by thermal oxidation of Sb₂S₃. *Bull. Mater. Sci.* **39**, 1801–1808 (2016). <https://doi.org/10.1007/s12034-016-1335-3>
50. R. Ben Belgacem, M. Chaari, A.F. Braña, B.J. Garcia, A. Matoussi, Structural, electric modulus and complex impedance analysis of ZnO/TiO₂ composite ceramics. *J. Am. Ceram. Soc.* **100**, 2045–2058 (2017). <https://doi.org/10.1111/jace.14725>
51. M. Chaari, R. Ben Belgacem, A. Matoussi, Impedance analysis, dielectric relaxation and modulus behaviour of ZnO-Sn₂O₃ ceramics. *J. Alloys Compd.* **726**, 49–56 (2017). <https://doi.org/10.1016/j.jallcom.2017.07.295>
52. M. Coşkun, Ö. Polat, F.M. Coşkun, Z. Durmuş, M. Çağlar, A. Türüt, The electrical modulus and other dielectric properties by the impedance spectroscopy of LaCrO₃ and LaCr_{0.90}Ir_{0.10}O₃ perovskites. *RSC Adv.* **8**, 4634–4648 (2018). <https://doi.org/10.1039/C7RA13261A>
53. M. Azizar Rahman, A.K.M. Akther, Hossain, Electrical transport properties of Mn–Ni–Zn ferrite using complex impedance

- spectroscopy. *Phys. Scr.* **89**, 025803 (2014). <https://doi.org/10.1088/0031-8949/89/02/025803>
54. Y. Ben Taher, N. Moutia, A. Oueslati, M. Gargouri, Electrical properties, conduction mechanism and modulus of diphosphate compounds. *RSC Adv.* **6**, 39750–39757 (2016). <https://doi.org/10.1039/C6RA05220G>

Publisher's Note Springer Nature remains neutral with regard to jurisdictional claims in published maps and institutional affiliations.